

An arginine ladder in OprP mediates phosphate-specific transfer across the outer membrane

Trevor F Moraes¹, Manjeet Bains², Robert E W Hancock² & Natalie C J Strynadka¹

The outer membrane protein OprP mediates the transport of essential phosphate anions into the pathogenic bacterium *Pseudomonas aeruginosa*. Here we report the crystallographic structure of trimeric OprP at 1.9-Å resolution, revealing an unprecedented 9-residue arginine ‘ladder’ that spans from the extracellular surface down through a constriction zone where phosphate is coordinated. Lysine residues coat the inner periplasmic surface, creating an ‘electropositive sink’ that pulls the phosphates through the eyelet and into the cell.

Pseudomonas aeruginosa is a Gram-negative bacterial pathogen and a leading cause of the nosocomial infections that particularly plague immunocompromised (HIV), burn and cystic fibrosis patients in hospitals and communities worldwide¹. Most bacteria, including *Pseudomonas*, react to environmental conditions of low phosphate by turning on a gene regulon that controls the expression of a number of phosphate-trafficking proteins^{2,3}. Outer membrane protein P (OprP) is a 48-kDa substrate-specific transporter whose expression is induced under conditions of low phosphate (<0.15 mM)^{4,5}. As part of the phosphate-starvation inducible transport system, OprP is involved in the high-affinity acquisition of the concentrations of phosphate that are crucial for *Pseudomonas* growth and proliferation⁴. Purification of OprP and subsequent analysis using planar lipid bilayer model membrane systems has indicated that the OprP channel contains a high-affinity binding site for phosphate, with a K_d of approximately 0.15 μM ⁶. These studies have also shown that, whereas

the channel is permeable to small anions in the absence of phosphate, their passage is blocked upon binding of phosphate to OprP. To understand the selective transport of phosphate by OprP, we have determined the 1.9-Å X-ray crystal structure of intact OprP in the presence of phosphate (see **Supplementary Methods** and **Supplementary Table 1** online for details).

The overall structure of OprP is shown in **Figure 1a,b** and a schematic representation of the topology in **Supplementary Figure 1** online. Consistent with previous insertion mutagenesis data⁷, each monomer of OprP adopts a 16-stranded antiparallel β -barrel structure with a strand tilt angle of 37° with respect to the barrel axis and a shear number of 16. The barrel is slightly elliptical (**Fig. 1b**). OprP forms a prominent trimer in solution, but unlike the many outer membrane porins (for example, PhoE and OmpF) in which the exoplasmic L2 loop contributes primarily to the integrity of the oligomer^{8,9}, OprP has an extended periplasmic N terminus that is involved in stabilizing the trimer through a ‘tricorn’-like strand exchange. This creates a ‘three-cornered hat’-shaped platform on the periplasmic face and also completes the fifteenth and sixteenth strands in the antiparallel β -barrel of each monomer (**Fig. 1b,c**). Other details of OprP’s relationship to the specific porin LamB¹⁰ and an anion porin, Omp32 (ref. 11), are described in the **Supplementary Discussion** online.

Three prominent elongated loop regions are evident in our OprP structure, the extracellular loops L3 and L5 and the periplasmic loop T7 (**Supplementary Fig. 1**). The L3 loop contains α -helices that extend deep into the cavity of the barrel and are responsible for the size and constriction of the pore, as seen in other membrane-spanning

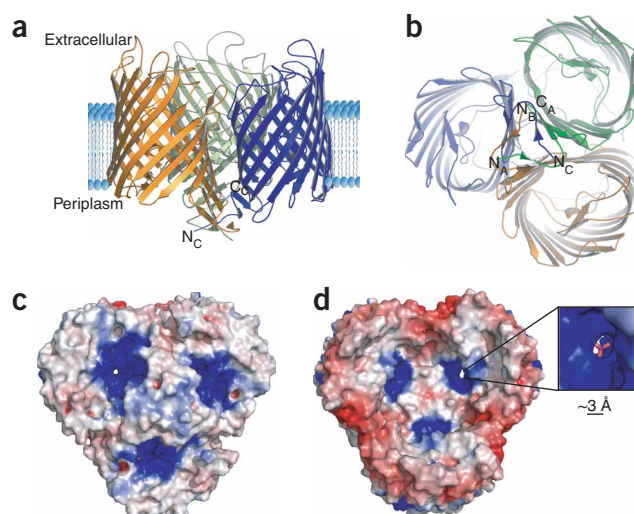


Figure 1 Overall structure of OprP. **(a)** OprP is shown in cartoon representation from a side view, with monomers shown in blue, green and orange and flanked by a cartoon lipid bilayer. **(b)** The tricorn N-terminal strands of OprP, viewed through the pore from the periplasmic space. N and C termini of monomers A, B and C are indicated. **(c,d)** Electrostatic surface potential, viewed from the periplasm **(c)** or from the extracellular space, slightly askew from the z-axis **(d)**; red, negative; blue, positive. **c** shows a uniform electronegative inner surface and a hydrophobic protrusion from the center of the three-fold noncrystallographic symmetry axis. **d** shows a glimpse of the narrowly constricted pore that is plugged by a phosphate anion (inset).

¹Department of Biochemistry and Molecular Biology and the Center for Blood Research, University of British Columbia, 2350 Health Sciences Mall, Vancouver, British Columbia V6T 1Z3, Canada. ²Center for Microbial Diseases and Immunity Research, University of British Columbia, 2259 Lower Mall Research Station, British Columbia V6T 1Z4, Canada. Correspondence should be addressed to N.C.J.S. (natalie@byron.biochem.ubc.ca).

Received 16 October; accepted 6 December; published online 24 December 2006; doi:10.1038/nsmb1189

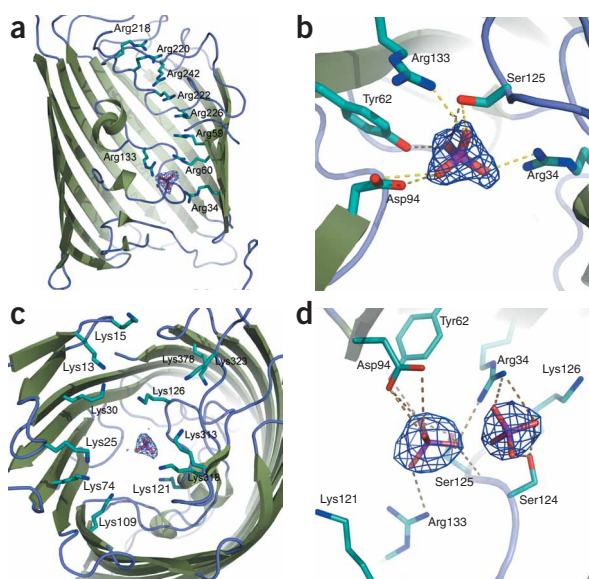


Figure 2 Mechanism of phosphate transport. (a) Cartoon of the arginine ladder located on the extracellular portion of each monomer. (b) Phosphate-binding plug located at the constriction zone, with $2F_o - F_c$ electron density for the phosphate residue contoured at 1.5σ . (c) Perioplasmic view of the channel, highlighting the lysine residues that compose the electropositive sink. (d) A second phosphate-binding site on the perioplasmic side of the constriction zone, depicted with $2F_o - F_c$ electron density (contoured at 1.8σ).

β -barrel proteins¹⁰. Uniquely in OprP, the L5 loop runs along the inner surface of the pore toward the center of the channel, creating an electropositive surface to attract anions (Fig. 1d). In L5, there are five arginine residues (Arg218, Arg220, Arg242, Arg226 and Arg226) that, together with two arginine residues in sheet B2 (Arg59 and Arg60), create a distinct, evenly spaced seven-step arginine ladder. The arginine guanidinium groups stack on one another $\sim 4 \text{ \AA}$ apart, creating an electropositive slide that propels the phosphate down the inner region of the exoplasmic surface toward the constriction zone (Fig. 1c,d). An additional two arginine residues (Arg133 in the L3 loop and Arg34 in the B1 sheet) complete the ladder (Fig. 2a).

On the extracellular surface of the OprP trimer, each monomer contributes to the formation of a giant funnel. The funnel has three separate electropositive arginine ladders that spiral down toward the point of greatest constriction ($\sim 3.5 \text{ \AA}$ across), near the perioplasmic face of the transporter. In our high-resolution electron density maps, we observed a well-ordered phosphate molecule trapped within each of the constriction zones of the OprP channel (Fig. 2b). The binding site is composed of the side chains of five residues: two protruding from the L3 constriction loop (Arg133 and Ser125) and single residues from strand B2 (Tyr62), strand B1 (Arg34) and the L2 loop (Asp94, the only negatively charged residue lining the interior surface of the channel). In addition, Lys121 also makes contact with the trapped phosphate in one of the three monomers and may serve as a ratchet (Supplementary Discussion). Together, these residues sequester phosphate anions at the narrowest point of the phosphate channel, effectively acting as a molecular plug localized approximately 23 \AA from the top of the arginine ladder (Arg216) at the extracellular face of OprP and 13 \AA from the edge of the electropositive funnel on the perioplasmic face (Lys313).

An obvious question from this analysis is how OprP manifests specificity for phosphate. At the narrowest point of the OprP porin, including the high-affinity phosphate-binding site, the channel has a diameter of $\sim 3.5 \text{ \AA}$ (Arg133-Asp94) over a length of $\sim 9 \text{ \AA}$ (made possible by the positioning of the L5, L3 and T7 loops, which is unique to OprP). There are several important physiological consequences associated with these loops that help facilitate specificity. First, larger molecules such as citrate cannot physically fit through the channel, as has been shown previously in solution using planar lipid bilayer assays¹². Second, by their specific chemical nature, the binding

residues at the phosphate-binding site discriminate against other anions of similar size, such as sulfate. The presence of Asp94 provides a hydrogen bond acceptor for the OH group on the monovalent form of phosphate, the expected form *in vivo*, given its pK_a values of ~ 2 and 7 . However, with two lone pairs and pK_a values both below 2 , the sterically similar sulfate is always effectively in the SO_4^{2-} divalent state under physiological conditions. As such, it cannot provide an equivalent hydrogen bond donor to the Asp94 residue (pK_a of side chain ~ 3.8), as does the preferentially bound phosphate. Our observations are supported by earlier planar lipid bilayer assays showing much lower affinities of OprP for sulfate ions than for phosphate ions, as well as pH dependency of phosphate binding, with pH values that support the monovalent form yielding higher affinities, and pH values that support the divalent form yielding lower affinities⁶. Finally, the high-affinity binding of phosphate at the constriction site, or plug, acts to reduce the movement of potentially deleterious smaller anions such as Cl^- and OH^- through this membrane channel, a mechanism of ion selection similar to that proposed for the voltage-gated potassium channel¹³.

On the perioplasmic side of the constriction site, each monomer of OprP is lined with 12 lysine residues that create a uniformly positively charged surface extending from the phosphate plug out toward the perioplasmic space (Fig. 1c and Fig. 2c), thereby acting as a marked electropositive sink to draw out phosphate from the channel. Earlier mutagenesis screens have shown that at least 2 of the 12 lysines, Lys126 and Lys74, affect the movement of anions through the OprP channel^{5,14}. Our structures show that Lys126 is relatively close to the phosphate plug, providing a path of electropositive potential necessary to attract phosphate out from the plug. This is supported by the observation of a second low-occupancy bound phosphate molecule located near (4.5 \AA) Lys126 (Fig. 2d). In contrast, Lys74 is located farther toward the perioplasmic surface ($\sim 20 \text{ \AA}$), where it may be contributing to the movement of phosphate away from the plug region and effectively lowering the local phosphate concentration near the plug. Together, the arginine ladder, the high-affinity phosphate-binding site and a lysine-filled perioplasmic electropositive sink within OprP enable this energy-independent channel to specifically transport phosphate anions across the outer membrane of *Pseudomonas aeruginosa*.

Accession codes. Protein Data Bank: Coordinates have been deposited with accession code 2O4V.

Note: Supplementary information is available on the Nature Structural & Molecular Biology website.

ACKNOWLEDGMENTS

We thank C. Egli and N. Martin for valuable discussion and the staff at the Advanced Light Source beamline 8.2.2 for data collection time and assistance. T.E.M. is supported by a Michael Smith Foundation for Health Research (MSFHR) postdoctoral fellowship. N.C.J.S. thanks the Howard Hughes International Scholar program and the Canadian Institutes of Health Research (CIHR) for funding and the Canadian Foundation for Innovation and the MSFHR for infrastructure support. R.E.W.H. thanks the CIHR for funding, the Canadian Cystic Fibrosis Foundation and the US Cystic Fibrosis Foundation. N.C.J.S. is a MSFHR Senior Scholar, CIHR Investigator and Howard Hughes Medical Institute International Scholar. R.E.W.H. is a CIHR Investigator.

AUTHOR CONTRIBUTIONS

M.B. purified and crystallized proteins; T.F.M. performed crystal optimization and X-ray structure determination; T.F.M., R.E.W.H. and N.C.J.S. were involved in the structural analysis and discussion.

COMPETING INTERESTS STATEMENT

The authors declare that they have no competing financial interests.

Published online at <http://www.nature.com/nsmb/>

Reprints and permissions information is available online at <http://npg.nature.com/reprintsandpermissions/>

1. National Nosocomial Infections Surveillance System. *Am. J. Infect. Control* **32**, 470–485 (2004).
2. Hancock, R.E. & Brinkman, F.S. *Annu. Rev. Microbiol.* **56**, 17–38 (2002).
3. Wanner, B.L. *J. C. Biochem.* **51**, 47–54 (1993).
4. Siehnel, R.J., Worobec, E.A. & Hancock, R.E. *Mol. Microbiol.* **2**, 347–352 (1988).
5. Sukhan, A. & Hancock, R.E. *J. Biol. Chem.* **271**, 21239–21242 (1996).
6. Benz, R., Egli, C. & Hancock, R.E. *Biochim. Biophys. Acta* **1149**, 224–230 (1993).
7. Sukhan, A. & Hancock, R.E. *J. Bacteriol.* **177**, 4914–4920 (1995).
8. Cowan, S.W. *et al. Nature* **358**, 727–733 (1992).
9. Schulz, G.E. *Biochim. Biophys. Acta* **1565**, 308–317 (2002).
10. Schirmer, T., Keller, T.A., Wang, Y.F. & Rosenbusch, J.P. *Science* **267**, 512–514 (1995).
11. Zachariae, U., Koumanov, A., Engelhardt, H. & Karshikoff, A. *Protein Sci.* **11**, 1309–1319 (2002).
12. Benz, R. & Hancock, R.E. *J. Gen. Physiol.* **89**, 275–295 (1987).
13. Doyle, D.A. *Eur. Biophys. J.* **33**, 175–179 (2004).
14. Hancock, R.E. & Benz, R. *Biochim. Biophys. Acta* **860**, 699–707 (1986).